



Deposition of Ag@AgCl onto Flower-Like BiOCl for Promoting the Degradation of Methyl Orange: The Narrow Bandgap and Surface Plasmon Resonance Effect

Sujing Zou¹ · Xiqiang Mao¹ · Lei Wu¹ · Yang Li¹ · Jun Li¹ · Jian Yang¹ · Ximei Fan¹

Received: 29 January 2024 / Revised: 22 April 2024 / Accepted: 8 May 2024 / Published online: 16 May 2024
© The Author(s), under exclusive licence to Korean Institute of Chemical Engineers, Seoul, Korea 2024

Abstract

Photocatalysis technology is considered as a most promising method to decompose organic pollutant since the inexhaustible solar energy and facile reaction condition. Herein, a series of flower-like Ag/AgCl/BiOCl photocatalysts are successfully synthesized via hydrothermal and photochemical deposition method. All the samples are investigated and characterized by X-Ray diffraction, Scanning electron microscopy, transmission electron microscope, ultraviolet–visible spectroscopy and Photoluminescence to insight into the microstructures and optical properties. During the photocatalytic degradation of Methyl orange experiments, the optimized Ag/AgCl/BiOCl sample prepared by photoreduction with 40 min exhibits the excellent photocatalytic performance. Under visible-light irradiation for 60 min, degradation rate of Methyl orange reaches 97%, which is 9.7, 6.1 and 4.6 times higher than that of AgCl, Ag/BiOCl and BiOCl, respectively. The UV–vis diffuse reflectance and Photoluminescence spectra of the Ag/AgCl/BiOCl photocatalyst verify that the enhanced photocatalytic activity is ascribed to its extended absorption range to visible-light region and the efficient separation efficiency of photogenerated carriers. In addition, the radical trapping experiment demonstrates that photogenerated hole and superoxide radicals play critical roles in the methyl orange degradation. The corresponding photocatalytic degradation mechanism is proposed that the excellent photocatalytic activity is attributed to the surface plasmon resonance effect of metallic Ag and heterojunction structure of Ag/AgCl/BiOCl photocatalysts.

Keywords Ag/AgCl/BiOCl · Flower-like microspheres · Visible-light degradation · Surface plasmon resonance

Introduction

Nowadays, climate change, environmental pollution and energy crisis etc. have aroused widespread global concern, and developing new and efficient technologies for environmental remediation has become increasingly important, especially for the wastewater treatment that containing metal ions, drugs, dyes or organic compounds. Photocatalysis is recognized as one of the most promising and efficient solutions for the

removal of organic pollutants since its advantages of high efficiency and low-energy consumption as well as free secondary pollution [1–3]. As the well-known photocatalyst, TiO₂ is still one of the most largely investigated and applied photocatalysts since its remarkable ultraviolet light activity, nontoxic and inexpensive. Unfortunately, its wide bandgap structure with about 3.2 eV limits the utilization efficiency of visible-light region, only can respond in the ultraviolet light ($\lambda < 380$ nm), which constitutes only 5% proportion of the solar spectrum [4]. Therefore, exploiting new visible-light response photocatalyst has been an urgent issue from the viewpoint of using solar energy to degradation organic pollutants. Ag/AgCl, as a typical plasmon photocatalyst, has attracted much attention for its relatively low cost and excellent visible-light region response [5, 6]. AgCl can effectively assist the photocatalytic activities and provide active chlorine atoms for photocatalytic reactions [7]. Ag nanoparticles (Ag NPs) possesses excellent visible-light response performance due to surface plasmon resonance (SPR) effect after exposure to visible-light. When Ag/AgCl is

✉ Jian Yang
jyang10619@swjtu.edu.cn

✉ Ximei Fan
xmfan@swjtu.edu.cn

¹ Key Laboratory of Advanced Technologies of Materials (Ministry of Education), School of Materials Science and Engineering, College of Materials Science and Engineering, Southwest Jiaotong University, Chengdu 610031, People's Republic of China

combined with other semiconductors, a strong interaction is generated on the heterojunction interface, which could promote better spatial separation of photogenerated carriers and thus enhance photocatalytic activity.

Bismuth-based semiconductors have attracted much attentions as photocatalysts for environmental security and remediation due to their unique electronic structure. For example, the BiOCl consists of $[\text{Bi}_2\text{O}_2]^{2-}$ inner layers sandwiched between two slabs of halogen ions, which could induce the formation of built-in electric field to accelerate the photogenerated carrier migration [8]. It is well known that bismuth oxychlorides possess good degradability for cationic dyes such as Rhodamine B (RhB) and methylene blue (MB), while poor degradation capacity for anions. This result is possibly ascribed to that BiOCl crystal is easily to form a nanostructure with exposed negative {001} facet [9, 10]. Therefore, enhancing the photocatalytic performance in the anionic dyes degradation with visible-light irradiation is still a challenge work. Among the reported various strategies, adjusting the exposed crystal surface to {010} facets can provide more active sites for dye absorption and photoelectron transfer [11]. On the other hand, the specific surface area also plays a critical role for separation efficiency of photogenerated carriers and the utilization of light. Many researchers devoted to synthesizing different BiOCl nanostructures including nanowires [12], nanobelts, nanosheets [13], nanoparticles [14], nanoflowers [15, 16], and hierarchical nanostructures [17]. The unique 3D hierarchical flower-like BiOCl nanosheets can provide a number of surface active sites. More importantly, it allows incident light to be reflected multiple times within the BiOCl nanosheets, thus improving the light utilization [18].

Therefore, a series of flower-like bismuth oxychloride heterojunction photocatalysts with Ag/AgCl were synthesized via multistep methods. The corresponding photocatalytic performance toward methylene orange (MO) degradation were evaluated under visible-light irradiation. The surface microstructure and composition of as-synthesized photocatalysts were characterized by XRD, SEM, TEM and X-Ray photoelectron spectroscopy (XPS) measurements. The optical properties were also investigated by UV-vis DRS, PL and valence band spectrum. At last, a reasonable photocatalytic reaction mechanism of the Ag/AgCl/BiOCl composite photocatalysts was proposed upon band energy analysis and radical trapping experiment.

Experimental

Materials

Bismuth nitrate pentahydrate ($\text{Bi}(\text{NO}_3)_3 \cdot 5\text{H}_2\text{O}$), Sodium chloride (NaCl), silver nitrate (AgNO_3),

Polyvinylpyrrolidone (PVP), Anhydrous ethanol ($\text{C}_2\text{H}_5\text{OH}$), Sodium hydroxide (NaOH) and Methylene orange (MO) were obtained from Chengdu Kelong Chemical Co. LTD (Chengdu, China). Standard solution of hydrochloric acid (0.1 M) was purchased from Aladdin Biochemical Technology Co. Ltd. (Shanghai, China). All chemical reagents were analytical pure and used without further purification.

Synthesis of Flower-Like BiOCl Microspheres

Flower-like BiOCl microspheres were synthesized through a hydrothermal method. In typical synthesis, 4 mmol of $\text{Bi}(\text{NO}_3)_3 \cdot 5\text{H}_2\text{O}$ and 0.1 g of PVP were added into 50 mL of deionized water with 5 mL ethanol solution and stirring until the solution was well mixed. Subsequently, 4 mL of NaCl solution (1 mol/L) was also dissolved into the above solution with constantly stirring. After the pH of prepared mixture solution was adjusted to 6.0 by NaOH (1.0 mol/L), the mentioned solution was poured into a 100 mL Teflon-lined stainless-steel autoclave and kept at 180 °C for 12 h. After naturally cooled to room temperature, the resultant samples were washed several times with deionized water and then dried overnight at 60 °C. And finally, the BiOCl catalysts were collected.

Fabrication of Ag/AgCl/BiOCl

As showed in Fig. 1, the ternary Ag/AgCl/BiOCl heterojunction materials were synthesized by a chemical deposition and photoreduction method. The procedure was as follows: 0.26 g of BiOCl were dispersed into 10 mL deionized water and then ultrasonicated for 10 min, denoted as solution A. 0.169 g of AgNO_3 was dissolved into 10 mL deionized water (0.1 mol/L), marked as solution B. Then, solution B was poured into solution A by dropwise addition. Next, 20 mL HCl solution (0.1 mol/L) was added to form AgCl particles which could be deposited on the BiOCl catalysts. The mixed solution was exposed to an ultraviolet light (20 W) for a certain time to generate Ag⁰ particles derived from AgCl. During the synthesis of Ag/AgCl/BiOCl, continuous magnetic stirring was carried out. Finally, the Ag/AgCl/BiOCl photocatalysts were recovered by centrifugation and rinsed with ultrapure-water and ethanol several times, then drying overnight at 60 °C. A battery of Ag/AgCl/BiOCl photocatalysts with different contents of Ag nanoparticles were synthesized by adjusting irradiation time (20 min, 40 min and 60 min) and the corresponding composites were named S1, S2 and S3, respectively. As a comparison, Ag/BiOCl catalyst was synthesized following a similar synthesis route with the exception of the adding of HCl.

Fig. 1 The schematic illustration of Ag/AgCl/BiOCl hetero-junction synthesis process



Characterization

X-Ray powder diffraction (XRD, Rigaku-Ultima IV, Japan) with Cu K α radiation was used to determine the crystal structures of the synthetic materials. The chemical makeup was characterized by X-Ray photoelectron spectroscopy (XPS, Thermo Scientific ESCALAB Xi, USA). The morphologies of the samples were analyzed by field emission Scanning electron microscopy (SEM, Hitachi-SU8220, Japan). To acquire pictures with elemental mapping, high-resolution transmission electron microscope (HRTEM, JEOL-2100F, Japan, accelerating voltage = 200 kV) and transmission electron microscopy (TEM, JEM-2100F, Japan) were conducted. To estimate the optical properties and energy band structure, UV–vis diffuse reflection spectroscopy (DRS) was carried out on a spectrophotometer (Unico-UV-2802, China) using BaSO₄ as the reference material. To evaluate the separation efficiency of electron–hole pairs, we used Photoluminescence spectroscopy (PL, Hitachi, F-4600, Japan). The total organic carbon (TOC) content was studied using Vario TOC Select German elements.

Photocatalytic Experiment

Methyl orange (MO) was selected to assess the photocatalytic activities. The light source the photocatalytic reaction needed is provided by a 350 W xenon lamp with a 420 nm cutoff filter. In this experiment, the catalyst (50 mg) was added to MO solution (50 mL, 10 mg/L), and then the mixture was placed in the dark for 30 min while stirring to equilibrium. During visible-light irradiation, 3 mL samples of the suspension were taken every 10 min. The supernatant was obtained by centrifugation, and then the remaining MO concentration was determined by a Unico UV-2802 Spectrophotometer. The photocatalytic degradation rate was measured by the following Equations:

$$D = (A_0 - A_t)/A_0 \times 100\% \quad (1)$$

where D refers to the photocatalytic degradation rate of MO; A₀ and A_t refer to the MO concentration initial and after the photocatalytic degradation experiment [19].

Active Species Trapping Experiments

In order to determine the dominated active species during the photocatalytic activity, three radicals including $\cdot\text{OH}$, h^+ and $\cdot\text{O}_2^-$ were indirectly detected with the addition of isopropyl alcohol (IPA), triethanolamine (TEOA), and benzoquinone (BQ) into the reaction system separately. The experimental conditions were similar to the former evaluation experiment, but before irradiation, different scavengers were inserted.

Results and Discussion

Structure, Morphologies and Chemical Compositions

XRD patterns of the BiOCl, AgCl and Ag/AgCl/BiOCl samples are displayed in Fig. 2. For pure BiOCl, the diffraction peaks at 12.0°, 27.9°, 33.5° and 46.7° were assigned to (001), (011), (012) and (020) lattice planes of BiOCl (JCPDS No.73-2060) [20], respectively. The result demonstrates the successful synthesis of BiOCl materials. Meanwhile, the diffraction peaks of AgCl at 27.91°, 32.21°, 46.21°, and 54.83° can correspond to (111), (200), (220) and (311) crystal planes of AgCl (JCPDS No.31-1238). After silver chloride and silver nanoparticles are deposited on the surface of BiOCl, the corresponding diffraction peaks belonging to AgCl and BiOCl are observed in the series of Ag/AgCl/BiOCl samples. However, there are no any diffraction peaks of Ag⁰, which is ascribed to the ultra-low content and ultra-fine size of photo-reduced Ag⁰.

XPS is performed to reveal the surface elemental composition and chemical states of as-prepared samples. As shown in Fig. 3a, the obvious peaks corresponding to Bi 4f, Cl 2p, C 1s, Ag 3d and O 1s are observed from the full survey scan

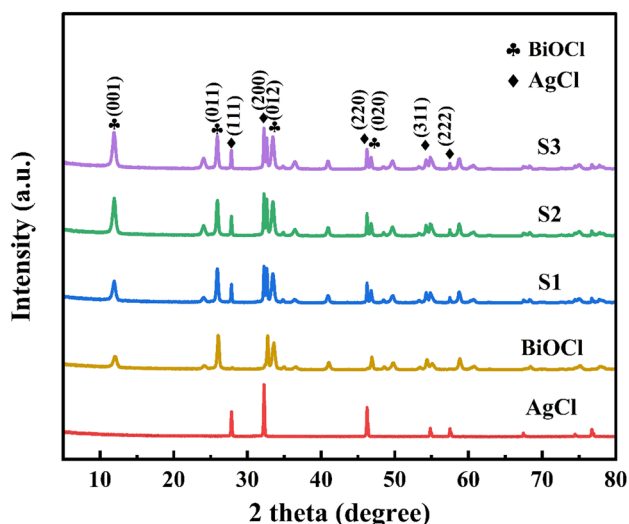


Fig. 2 XRD patterns of as-synthesized samples

spectrum of S2 samples, which is consistent with expected. There are two peaks at 197.7 eV and 199.3 eV in the high-resolution Cl 2p spectrum in Fig. 3b, which are assigned to the Cl 2p_{1/2} and Cl 2p_{3/2}, respectively [21]. For comparison of the pure BiOCl, the binding energy of Cl 2p in Ag/AgCl/BiOCl presents significantly positive shift, showing that the electron transfer is occurred from BiOCl to AgCl with the

strong interaction after contacted. In addition, the peaks of high-resolution Bi 4f in Fig. 3c at 159.0 and 164.3 eV are ascribed to Bi 4f_{7/2} and Bi 4f_{5/2}, respectively [22]. The obvious increase of binding energy in Ag/AgCl/BiOCl relative to pure BiOCl also verifies the electron transfer from BiOCl to Ag/AgCl/BiOCl after contacted, suggesting the formation of heterojunction between Ag/AgCl and BiOCl. Furthermore, the high-resolution O 1s spectrum in Fig. 3d can be deconvoluted into three different peaks at 529.7, 531.1 and 532.4 eV, which are attributed to the characteristic peaks of Bi–O bond, H₂O and adsorbed O₂ on the surface of compounds, respectively. For the high-resolution Ag 3d spectra in Fig. 3e, two strong peaks at 367.1 and 373.2 eV are assigned to Ag 3d_{5/2} and Ag 3d_{3/2}, which indicates the appearance of Ag⁺ cation. Compared with that of AgCl, the binding energy presents negative shift in Ag/AgCl/BiOCl, indicating that the Ag/AgCl obtains electrons after formation heterojunction between Ag/AgCl and BiOCl. What's more, the peaks at 373.6 and 367.5 eV belong to Ag 3d_{3/2} and Ag 3d_{5/2} of Ag⁰ metal [23, 24]. The above results demonstrate the strong interaction between AgCl/BiOCl after contacted as well as the existing of Ag⁰ metal, indicating the successful synthesis of Ag/AgCl/BiOCl heterojunctions.

SEM and TEM are carried out to investigate the morphology and internal structural properties. As shown in Fig. 4a and b, flower-like BiOCl microspheres stacked with nanosheets are observed, suggesting the large specific

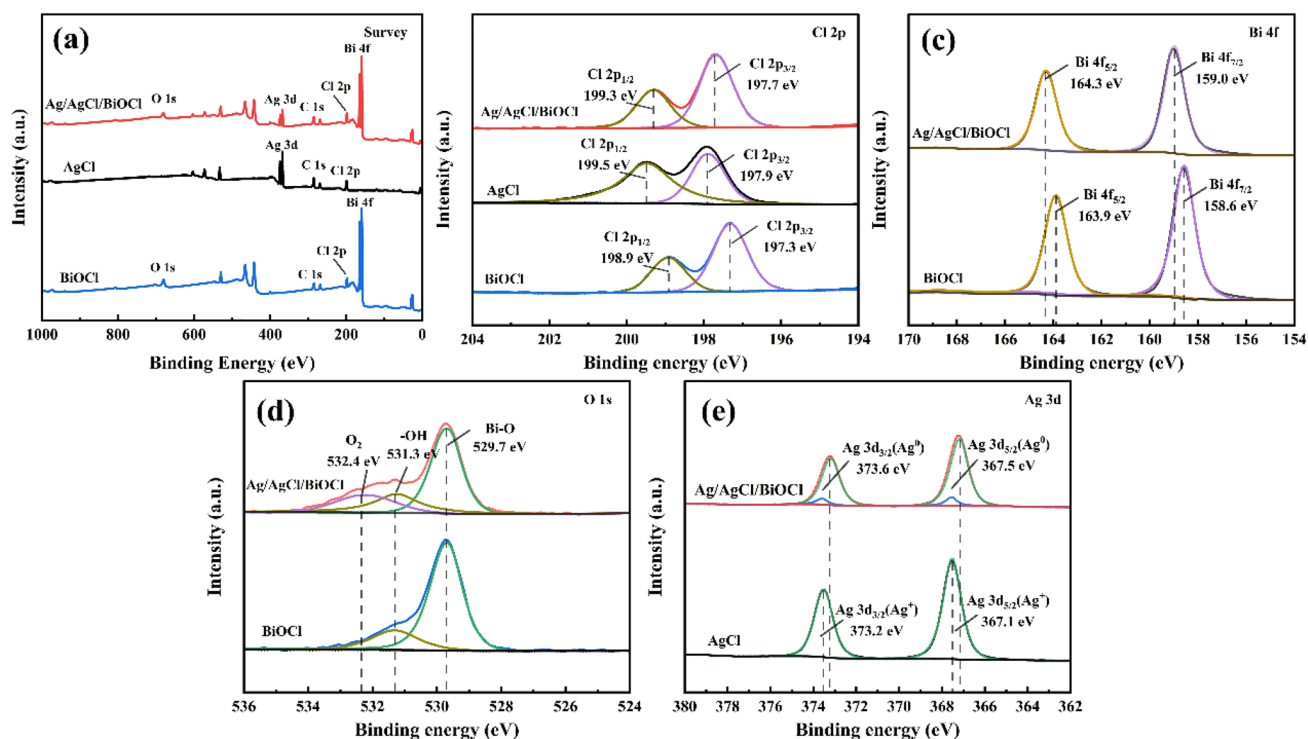


Fig. 3 a XPS survey spectra of BiOCl and S2 sample; b–e the high-resolution XPS spectra of Cl 2p, Bi 4f, O 1s, and Ag 3d

surface area and abundant active sites. Figure 4c shows the microsphere morphology of AgCl, prepared by chemical deposition. Combining SEM and subsequent TEM images, it could figure out that the primary morphology features of the samples would not change significantly after AgCl deposited on the surface of BiOCl in Fig. 4d and e as well as the following photo-reducing of AgCl to Ag nanocluster. The HRTEM image of Ag/AgCl/BiOCl in Fig. 4f displays three kinds of lattice spacings of 0.274, 0.235 and 0.277 nm, which fit well with the (013) face for BiOCl, (111) face for Ag and (200) face for AgCl, respectively [25].

According to element mapping images in Fig. 5, O, Cl, Bi and Ag elements are uniformly distributed in the sample, further reveals the constitute of Ag/AgCl/BiOCl.

Photocatalytic Activity and Durability for MO Degradation

To evaluate the photocatalytic performance of as-prepared samples, the organic dye MO is served as the target pollutant to investigate the degradation rate under visible-light (> 420 nm) irradiation. First of all, the MO solution with photocatalysts is placed in dark conditions for 30 min to ensure the adsorption–desorption equilibrium. As showed in Fig. 6a, the pure BiOCl, AgCl and Ag/BiOCl exhibit poor photocatalytic activities since their slightly decrease of MO concentration. Interestingly, the Ag/AgCl/BiOCl samples display excellent photocatalytic degradation performance with significantly decline of MO concentration. After 60 min irradiation under visible light, the sample of S2 presents superior photocatalytic activities with 97% of MO degradation rate to those of S1 (86%) and S3 (90%) samples. The results suggest that Ag/AgCl/BiOCl plasmon resonance system could make full use of visible light and thus improve

Fig. 4 SEM images of **a** and **b** BiOCl, **c** AgCl and **d** Ag/AgCl/BiOCl; **e** TEM image of Ag/AgCl/BiOCl; **f** HRTEM image of Ag/AgCl/BiOCl and the corresponding lattice fringes for Ag⁰, AgCl and BiOCl species

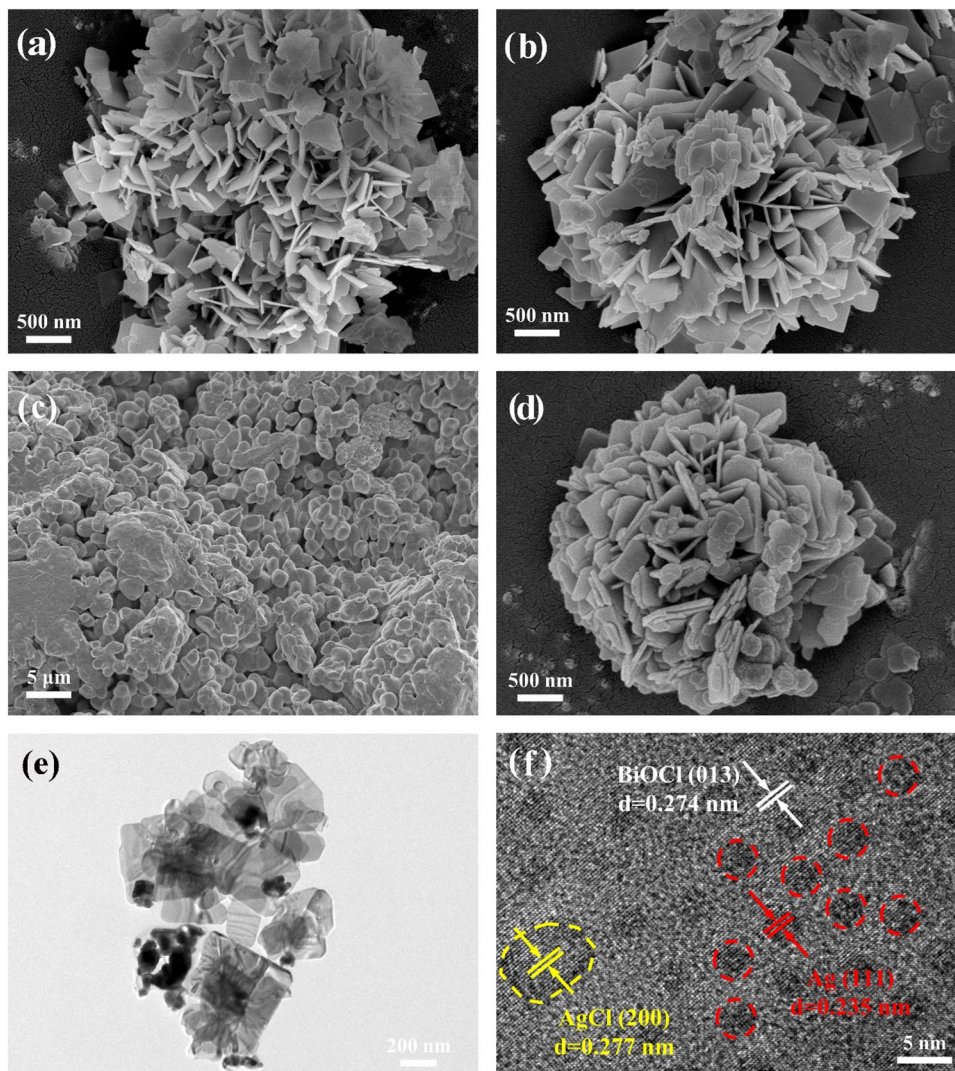
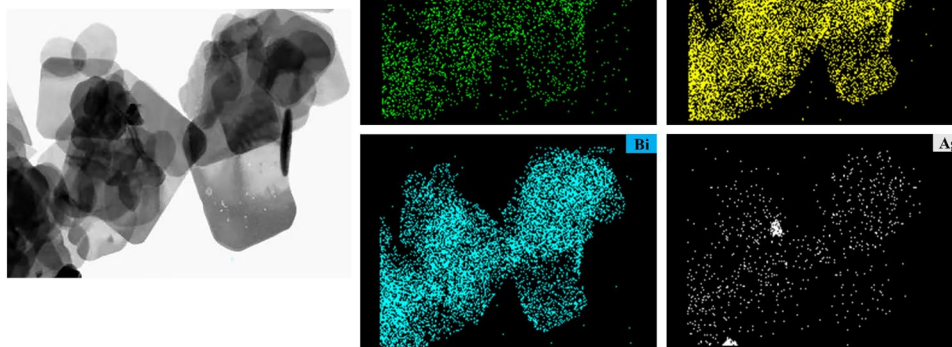


Fig. 5 The corresponding element mapping images of S2 sample



the degradation efficiency of organic dyes. In addition, the amount of Ag regulated by controlling the photo-irradiation time could affect the photocatalytic performance. A small amount of Ag NPs could not significantly improve the light response, while excessive Ag NPs would agglomerate and occupy the active site on the surface of AgCl and BiOCl, resulting in a decrease of photocatalytic activity. In Fig. 6b, the degradation rate constant (K) is achieved through a pseudo-first order kinetic model [26, 27]. The K value of S2 is about 0.05095, better than the other two samples. Notably, it was 35 and 25 times higher than that of AgCl and BiOCl. As Fig. 6c showed, the absorption intensity peak was found to be decreased due to the lowering dye concentration while increasing the irradiation time. To determine the mineralization degree of the MO dyes, TOC analyses were performed on dispersions at different visible-light irradiation times [28]. In Fig. 6d, the Ag/AgCl/BiOCl(S2) exhibited nearly 60% decomposition for MO after 60 min in visible-light irradiation. It showed that most of the methyl orange dye molecules were mineralized to H_2O and CO_2 under visible-light irradiation [29]. It further proves that Ag/AgCl/BiOCl possesses excellent photocatalytic performance. The stability and durability of photocatalytic materials are also important keys of their practical application in organic dyes degradation. The S2 sample are collected after each MO degradation experiment and washed by ethanol, then dried for the next evaluation experiment. As showed in Fig. 6e, after four consecutive cycles, the MO degradation rate of S2 sample still remains at 92%, which indicates that the sample have excellent photocatalytic durability. Figure 6f shows the crystal structure of S2 sample before and after the cycle experiments. There is no significant change after multiple illuminations, indicating its good structure stability.

Table 1 shows the catalytic performance of several bismuth oxychloride nanomaterials. What we can see that the bismuth oxide chloride composite has a certain degradation effect on common dyes such as MO, MB and RhB under

different light sources. Obviously, one can see that the catalyst prepared in this experiment has excellent catalytic performance.

Optical Properties

PL spectroscopy is performed to elucidate the photogenerated carrier recombination rate of photocatalytic materials. Generally, the PL emission peak intensity is proportional to the electron/hole recombination rate. The lower PL intensity corresponds to high photocatalytic activity, indicating that more electrons and holes can participate in the process of activating free radicals or directly oxidizing the pollutants adsorbed on the surface [36]. As shown in Fig. 7, the pure BiOCl displays a higher PL-diffraction peak compared to those of Ag/AgCl/BiOCl photocatalysts, which reveals that pristine BiOCl has a higher carrier recombination rate. Notably, the S2 sample exhibits a lowest PL emission peak intensity, indicating its outstanding carrier separation efficiency as well as superior photocatalytic activities in MO degradation.

To study the light absorption properties and the band gaps of pure BiOCl, AgCl, and Ag/AgCl/BiOCl photocatalysts, the UV–vis diffuse reflectance spectra (UV–vis DRS) analysis is performed. As shown in Fig. 8a, the pure BiOCl has no absorbance in the visible-light range. When composited with Ag/AgCl, the absorption intensities of Ag/AgCl/BiOCl photocatalysts become stronger in the whole light region, which may be ascribed to SPR effect of metallic Ag nanoparticles [37]. Based on the UV–vis absorption results, the band gaps (E_g) of the synthesized samples are calculated with the empirical equation [38, 39]:

$$(\alpha h\nu)^n = k(h\nu - E_g) \quad (2)$$

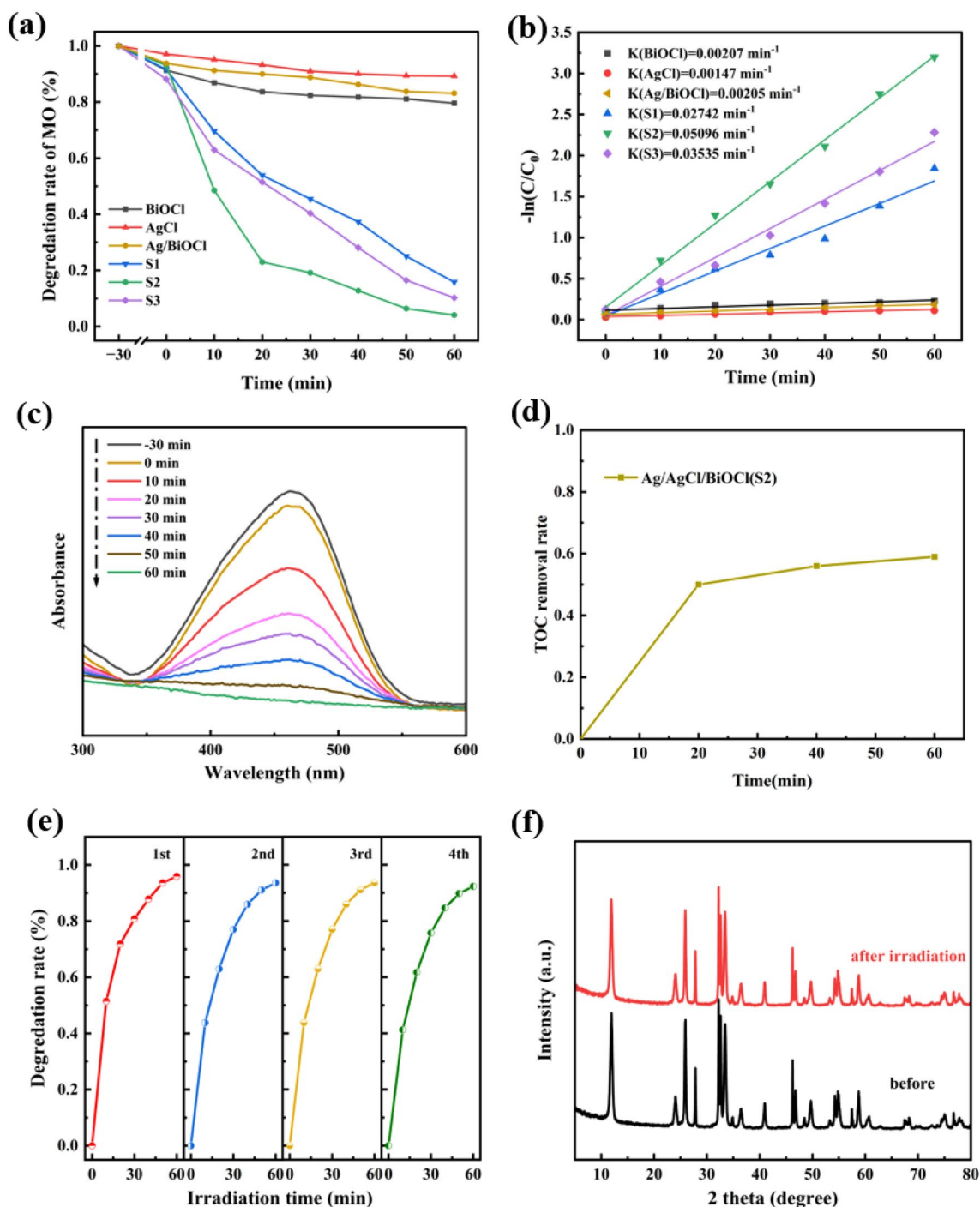


Fig. 6 The photocatalytic activities of as-synthesized samples toward MO degradation under visible-light irradiation. **a** MO removal rate of prepared samples in 60 min irradiation; **b** the corresponding pseudo-first-order kinetics of MO degradation; **c** the spectrum evolution of

MO over the S2 sample; **d** TOC degradation in the system of S2 with visible light; **e** the cycling test for photodegradation MO over S2 photocatalyst; **f** the XRD pattern of S2 sample before and after cycling test

As a result, the band gaps (Fig. 8b) values of BiOCl, AgCl, S1, S2 and S3 are 3.21 eV, 3.07 eV, 2.85 eV, 2.89 eV and 2.92 eV, respectively. The photocatalytic behavior of as-synthesized photocatalysts is associated with its band structure, where VB position of these materials is calculated

by XPS technique (Fig. 8c). The $E_{\text{VB-XPS}}$ values of BiOCl, AgCl and Ag/AgCl/BiOCl (S2) are 3.02, 2.82 and 2.50 eV, respectively, which is consistent with that reported for this material. The valence band can be calculated by the following formula:

Table 1 Comparative study on several bismuth oxychloride nanomaterials in photocatalytic degradation of different dyes with the earlier reported literature

Photocatalyst	Dye types	Efficiency/time	Light source	Wavelength	References
BiOCl/BiFeO ₃	RhB	92%/150 min	A 300 W Xe lamp	> 400 nm	[30]
Fe ³⁺ /BiOCl	MO	99%/80 min	A 250 W Xe lamp	Sunlight	[31]
BiOCl-TiO ₂	MB	80%/180 min	Tungsten bulb	Sunlight	[32]
BiOCl/BiOF	MO	95%/70 min	A 300 W Xe lamp	Sunlight	[33]
CdS QDs/BiOCl	MO	60%/120 min	A 500 W Xe lamp	Sunlight	[34]
BiOI/BiOCl	MB	99%/120 min	A 350 W Xe lamp	> 420 nm	[35]
Ag/AgCl/BiOCl	MO	97%/60 min	A 350 W Xe lamp	> 420 nm	This work

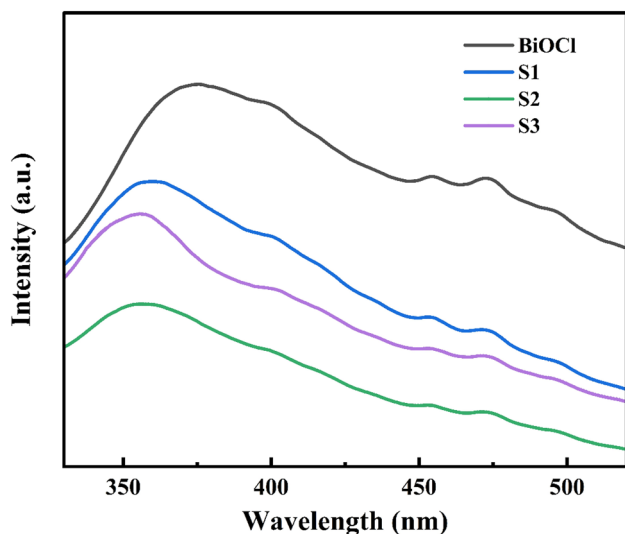
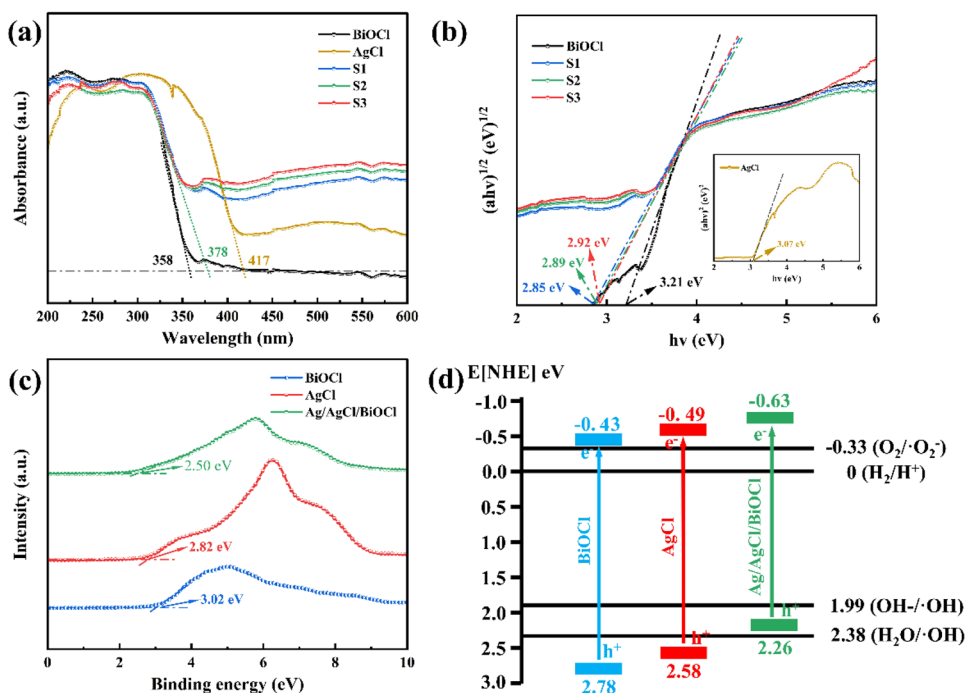


Fig. 7 PL spectra of pure BiOCl, S1, S2 and S3

Fig. 8 **a** UV-vis DRS spectra and **b** corresponding bandgap values of the prepared samples, predicted by the plot of $(\alpha h\nu)^{1/2}$ vs. photo energy; XPS valence band spectra **c** the band positions **d** of BiOCl, AgCl, and S2 sample



$$E_{\text{VB-NHE}} = \varphi + E_{\text{VB-XPS}} - 4.44 \quad (3)$$

φ of 4.20 eV: the electron work function of the analyzer [40]. Therefore, the $E_{\text{VB-NHE}}$ value of BiOCl, AgCl and Ag/AgCl/BiOCl (S2) are 2.78, 2.58 and 2.26 V (vs. NHE). Furthermore, the conduction band minimum (CB_M) is calculated from the equation [41]

$$E_{\text{CBM}} = E_{\text{VBM}} - E_g \quad (4)$$

The band positions of BiOCl, AgCl, and Ag/AgCl/BiOCl(S2) are plotted in Fig. 8d.

Mechanism of Ag/AgCl/BiOCl Heterojunction

Generally speaking, the active species mainly include h^+ , $\cdot\text{OH}$ and $\cdot\text{O}_2^-$ in the photocatalytic reaction. It could be indirectly detected by adding corresponding scavengers. The IPA, TEOA and BQ were used in the photocatalytic

process to trap the radicals ($\cdot\text{OH}$), (h^+), and ($\cdot\text{O}_2^-$) radicals, respectively [42, 43]. In Fig. 9a, with IPA adding to, the degradation efficiency of MO is not affected, indicating that $\cdot\text{OH}$ radicals are not the main active species involved in the reaction. On the contrary, the photocatalytic degradation rate of MO is significantly reduced after the addition of BQ. It showed that $\cdot\text{O}_2^-$ radicals took part in the MO degradation. Furthermore, with the addition of TEOA, the photocatalytic degradation rates of MO dramatically decrease. It suggesting that the h^+ are the predominated active species. We added the rate constant for each quencher to reactive species in Fig. 9b. It could be clearly observed that the h^+ and $\cdot\text{O}_2^-$ are the predominated active species rather than $\cdot\text{OH}$ during the photocatalytic reaction. In addition, it is reported that the chlorine ion on the surface of BiOCl could be oxidized to chlorine radical [44, 45]. These chlorine free radicals would participate in the degradation reaction, leading to the enhancement of photocatalytic performance [46].

Based on the experimental results and band structure analysis, a possible photocatalytic mechanism of Ag/AgCl/BiOCl for enhancing the photocatalytic performance is proposed and displayed in Fig. 10. Under the irradiation of visible light with >420 nm wavelength, the electron in the VB of BiOCl and AgCl could not be excited to CB since their wide bandgap. Owing to the SPR effect of Ag on the surface of Ag/AgCl/BiOCl, the visible light are absorbed by Ag and thus the electron-hole pairs are generated via the SPR effect of metallic Ag. The increased electrons located on the surface of Ag NPs are further transferred to CB of AgCl and further to CB of BiOCl since their relatively lower potential. This kind of carrier transfer path can effectively restrain recombination of photogenerated electron-hole pairs and improve the carrier lifetime. At last, the transferred CB electrons migrate to the surface of BiOCl to reduce the absorbed

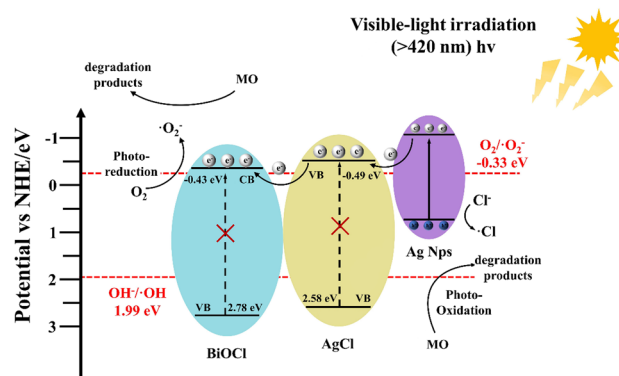


Fig. 10 The proposed band structure model and the possible photogenerated carriers transfer route for the MO degradation over Ag/AgCl/BiOCl

O_2 to $\cdot\text{O}_2^-$ radicals since the enough negative CB potential (-0.39 V vs. NHE) to $\text{O}_2/\cdot\text{O}_2^-$ (-0.03 V vs. NHE). Meanwhile, the retained hole in Ag could directly oxidize the organic pollutant molecules. This carrier transfer mechanism is consistent with the results mentioned above that h^+ , $\cdot\text{O}_2^-$ and $\cdot\text{Cl}$ are the main active species involved in the reaction. Moreover, such an electron transfer process could effectively reduce the recombination rate. Ag/AgCl/BiOCl heterojunction exhibits superior photocatalytic performance on the MO degradation with visible-light irradiation.

Conclusion

In summary, the flower-like Ag/AgCl/BiOCl photocatalysts have been successfully constructed by in-situ loading Ag/AgCl nanoparticles on BiOCl with the aid of a

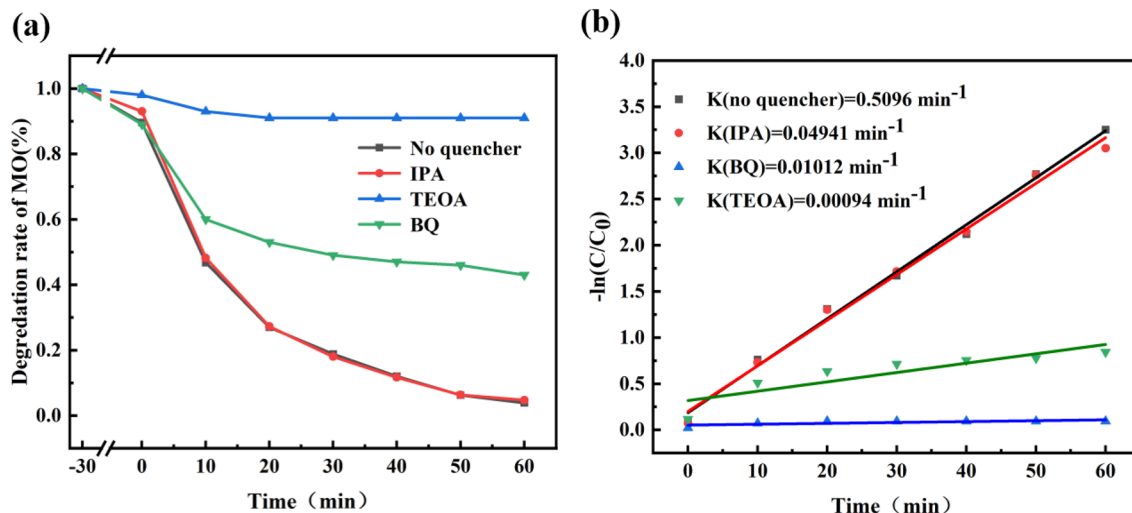


Fig. 9 **a** The effect of different quenchers on the photocatalytic degradation of MO; **b** apparent rate constants for various of quenchers

photoreduction precipitation technique. A series of ternary Ag/AgCl/BiOCl photocatalysts with various UV-light irradiation time are synthesized. The optimized Ag/AgCl/BiOCl photocatalyst prepared by about 40 min UV irradiation exhibits preferable photocatalytic activity for MO degradation rate under visible-light irradiation. The characterization results reveal that the improved absorption range of Ag/AgCl/BiOCl photocatalyst, especially in the visible-light region and the robust separation efficiency of electron–hole pairs are the mainly reasons to obtain excellent photocatalytic degradation performance. The active species trapping experiments show that h^+ and $\bullet O_2^-$ are the predominate active species in the MO decomposing. The proposed mechanism indicates that Ag NPs play crucial roles in the generation of electron–hole pairs under visible-light irradiation. In addition, the carrier transfer path is in according with experiment results. More importantly, this strategy can be widely applied to the environmental purification of organic pollutants in sewage disposal field.

Acknowledgements This work was supported by the National Natural Science Foundation of China (Grant No. 52102308), the Sichuan Science and Technology Program (2023YFG0249). In addition, we would like to thank the Analytical and Testing Center of Southwest Jiaotong University for supporting the XRD, SEM, TEM, Raman, etc. measurements.

Author Contributions S.Z. fabricated the samples and wrote the main manuscript. X.M. and L.W. helped with the XPS measurement. Y.L. and J.L. analyzed data and revised the main manuscript. J.Y. and X.F. conceptualized and supervised the research. All authors have read and agreed to the submitted version of the manuscript.

Funding This article is funded by National Natural Science Foundation of China, No. 52102308, jian yang, Sichuan Province Science and Technology Support Program, 2023YFG0249, jian yang.

Data Availability All data in this paper are available from the author upon reasonable request.

Declarations

Conflict of Interest Authors declare no conflict of interest.

References

1. W.S. Koe, J.W. Lee, W.C. Chong et al., An overview of photocatalytic degradation: photocatalysts, mechanisms, and development of photocatalytic membrane. *Environ. Sci. Pollut. Res. Int.* **27**, 2522–2565 (2020). <https://doi.org/10.1007/s11356-019-07193-5>
2. D.T. Ruziwa, A.E. Oluwalana, M. Mupa et al., Pharmaceuticals in wastewater and their photocatalytic degradation using nano-enabled photocatalysts. *J. Water Process. Eng.* **54**, 103880 (2023). <https://doi.org/10.1016/j.jwpe.2023.103880>
3. P. Eghbali, A. Hassani, S. Wacławek et al., Recent advances in design and engineering of MXene-based catalysts for photocatalysis and persulfate-based advanced oxidation processes: a state-of-the-art review. *Chem. Eng. J.* **480**, 147920 (2023). <https://doi.org/10.1016/j.cej.2023.147920>
4. Y. Ide, N. Inami, H. Hattori et al., Remarkable charge separation and photocatalytic efficiency enhancement through interconnection of TiO₂ nanoparticles by hydrothermal treatment. *Angew. Chem. Int. Ed. Engl.* **55**(11), 3600–3605 (2016). <https://doi.org/10.1002/ange.201510000>
5. F. Wang, X. Liang, P. Wang et al., Ag/AgCl as an efficient plasmonic photocatalyst for greenhouse gaseous methane oxidation. *J. Environ. Chem. Eng.* **9**(6), 106435 (2021). <https://doi.org/10.1016/j.jece.2021.106435>
6. L. Song, Zhao X Zhang S, Preparation and photocatalytic activity of carbon dot/Ag/AgCl. *Appl. Organomet. Chem.* **33**(9), e5019 (2019). <https://doi.org/10.1002/aoc.5019>
7. Y. Dai, Y. Liu, J. Kong et al., High photocatalytic degradation efficiency of oxytetracycline hydrochloride over Ag/AgCl/BiVO₄ plasmonic photocatalyst. *Solid State Sci.* **96**, 105946 (2019). <https://doi.org/10.1016/j.solidstatesciences.2019.105946>
8. J. Di, J. Xia, H. Li et al., Bismuth oxyhalide layered materials for energy and environmental applications. *Nano Energy* **41**, 172–192 (2017). <https://doi.org/10.1016/j.nanoen.2017.09.008>
9. H. Tang, T. Ju, Y. Dai et al., Synthesis and photocatalytic performance of BiOCl/graphene composite with tight interfacial contact and highly exposed (001) facets. *Appl. Organomet. Chem.* **36**(2), e6526 (2022). <https://doi.org/10.1002/aoc.6526>
10. S. Ning, X. Shi, H. Zhang et al., Reconstructing dual-induced 0 0 1 facets bismuth oxychloride nanosheets heterostructures: an effective strategy to promote photocatalytic oxygen evolution. *Solar RRL.* **3**(5), 1900059 (2019). <https://doi.org/10.1002/solr.201900059>
11. L. Zhang, C.G. Niu, G.X. Xie et al., Controlled growth of BiOCl with large 010 facets for dye self-photosensitization photocatalytic fuel cells application. *ACS Sustain. Chem. Eng.* **5**(6), 4619–4629 (2017). <https://doi.org/10.1021/acssuschemeng.6b03150>
12. X. Liao, X. Lan, N. Ni et al., Bismuth oxychloride nanowires for photocatalytic decomposition of organic dyes. *ACS Appl. Nano Mater.* **4**(4), 3887–3892 (2021). <https://doi.org/10.1021/acsnm.1c00288>
13. B. Zhang, J. Zhang, R. Duan et al., BiOCl nanosheets with periodic nanochannels for high-efficiency photooxidation. *Nano Energy* **78**, 105340 (2020). <https://doi.org/10.1016/j.nanoen.2020.105340>
14. G. Sui, Y. Zhang, J. Li et al., Modification of hollow BiOCl/TiO₂ nanotubes with phosphoric acid to enhance their photocatalytic performance. *Korean J. Chem. Eng.* **39**(4), 986–996 (2022). <https://doi.org/10.1007/s11814-021-0997-8>
15. X. Zhang, L. Yuan, F. Liang et al., Water-assisted synthesis of shape-specific BiOCl nanoflowers with enhanced adsorption and photosensitized degradation of rhodamine B. *Environ. Chem. Lett.* **18**, 243–249 (2020). <https://doi.org/10.1007/s10311-019-00929-2>
16. A. Kuila, P. Saravanan, D. Bahnemann et al., Novel Ag decorated, BiOCl surface doped AgVO₃ nanobelt ternary composite with Z-scheme homojunction-heterojunction interface for high prolific photo switching, quantum efficiency and hole mediated photocatalysis. *Appl. Catal. B Environ.* **293**, 120224 (2021). <https://doi.org/10.1016/j.apcatb.2021.120224>
17. H.Y. Hao, Y.Y. Xu, P. Liu et al., BiOCl nanostructures with different morphologies: tunable synthesis and visible-light-driven photocatalytic properties. *Chin. Chem. Lett.* **26**(1), 133–136 (2015). <https://doi.org/10.1016/j.ccllet.2014.11.022>
18. B. Sarwan, A.D. Acharya, S. Kaur et al., Visible light photocatalytic deterioration of polystyrene plastic using supported BiOCl nanoflower and nanodisk. *Eur. Polym. J.* **134**, 109793 (2020). <https://doi.org/10.1016/j.eurpolymj.2020.109793>
19. S.S. Hossain, M. Tarek, T.D. Munusamy et al., Facile synthesis of CuO/CdS heterostructure photocatalyst for the effective degradation of dye under visible light. *Environ. Res.* **188**, 109803 (2020). <https://doi.org/10.1016/j.envres.2020.109803>

20. L. Zhang, C.G. Niu, X.F. Zhao et al., Ultrathin BiOCl single-crystalline nanosheets with large reactive facets area and high electron mobility efficiency: a superior candidate for high-performance dye self-photosensitization photocatalytic fuel cell. *ACS Appl. Mater. Interfaces* **10**(46), 39723–39734 (2018). <https://doi.org/10.1021/acsami.8b14227>
21. S. Gong, F. Rao, J. Xu et al., A self-stable plasmonic Ag/p-Ag₂O/n-BiOCl heterojunction with enhanced photocatalytic CO₂ reduction. *Mater. Today Phys.* **2023**, 101189 (2023). <https://doi.org/10.1016/j.mtphys.2023.101189>
22. Z. Chen, Y. Ma, W. Chen et al., Enhanced photocatalytic degradation of ciprofloxacin by heterostructured BiOCl/Ti₃C₂T_x MXene nanocomposites. *J. Alloys Compd.* **950**, 169797 (2023). <https://doi.org/10.1016/j.jallcom.2023.169797>
23. Q. Li, G. Duan, J. Luo et al., Ultrasonic-assisted synthesis of plasmonic Z-scheme Ag/AgCl/WO₃-nanoflakes photocatalyst in geothermal water with enhanced visible-light photocatalytic performance. *J. Energy Chem.* **27**(3), 826–835 (2018). <https://doi.org/10.1016/j.jechem.2017.05.011>
24. D.O. Adenuga, S.M. Tichapondwa, E.M.N. Chirwa, Facile synthesis of a Ag/AgCl/BiOCl composite photocatalyst for visible-light-driven pollutant removal. *J. Photochem. Photobiol. A Chem.* **401**, 112747 (2020). <https://doi.org/10.1016/j.jphotochem.2020.112747>
25. L. Ye, J. Liu, C. Gong et al., Two different roles of metallic Ag on Ag/AgX/BiOX (X= Cl, Br) visible light photocatalysts: surface plasmon resonance and Z-scheme bridge. *ACS Catal.* **2**(8), 1677–1683 (2012). <https://doi.org/10.1021/cs300213m>
26. C.L. Yu, L.F. Wei, J.C. Chen et al., Novel AgCl/Ag₂CO₃ heterostructured photocatalysts with enhanced photocatalytic performance. *Rare Met.* **35**, 475–480 (2016). <https://doi.org/10.1007/s12598-014-0431-z>
27. M. Durai, D. Chauhan, M. Durai et al., Layered KTO/BiOCl nanostructures for the efficient visible light photocatalytic degradation of harmful dyes. *Chemosphere* **306**, 135659 (2022). <https://doi.org/10.1016/j.chemosphere.2022.135659>
28. T. Kanagaraj, S. Thiripuranthagan, Photocatalytic activities of novel SrTiO₃-BiOBr heterojunction catalysts towards the degradation of reactive dyes. *Appl. Catal. B Environ.* **207**, 218–232 (2017). <https://doi.org/10.1016/j.apcatb.2017.01.084>
29. K.R.S. Devi, S. Mathew, R. Rajan et al., Biogenic synthesis of g-C₃N₄/Bi₂O₃ heterojunction with enhanced photocatalytic activity and statistical optimization of reaction parameters. *Appl. Surf. Sci.* **494**, 465–476 (2019). <https://doi.org/10.1016/j.apsusc.2019.07.125>
30. P. Fourmont, S.G. Cloutier, Screen-printed p–n BiOCl/BiFeO₃ heterojunctions for efficient photocatalytic degradation of Rhodamine B. *RSC Adv.* **12**(38), 24868–24875 (2022). <https://doi.org/10.1039/d2ra03308a>
31. R. Rameshbabu, G. Pecchi, E.J. Delgado et al., BiOCl ultrathin nanosheets modified with Fe³⁺ for enhanced visible light driven photocatalytic activity. *J. Photochem. Photobiol. A.* **411**, 113211 (2021). <https://doi.org/10.1016/j.jphotochem.2021.113211>
32. V.G. Warriar, A. Nizam, G. Nagaraju, Highly efficient photocatalytic conversion of amine to amide and degradation of methylene blue using BiOCl–TiO₂ nano heterostructures. *J. Inorg. Organomet. Polym.* **30**, 3143–3157 (2020). <https://doi.org/10.1007/s10904-020-01471-3>
33. J. Cheng, L. Frezet, P. Bonnet et al., Preparation and photocatalytic properties of a hierarchical BiOCl/BiOF composite photocatalyst. *Catal. Lett.* **148**, 1281–1288 (2018). <https://doi.org/10.1007/s10562-018-2296-5>
34. J. Pan, J. Liu, S. Zuo et al., Synthesis of cuboid BiOCl nanosheets coupled with CdS quantum dots by region-selective deposition process with enhanced photocatalytic activity. *Mater. Res. Bull.* **103**, 216–224 (2018). <https://doi.org/10.1016/j.materresbull.2018.03.043>
35. Y. Zhong, Y. Liu, S. Wu et al., Facile fabrication of BiOI/BiOCl immobilized films with improved visible light photocatalytic performance. *Front. Chem.* **6**, 58 (2018). <https://doi.org/10.3389/fchem.2018.00058>
36. K. Zhang, Y. Liu, J. Deng et al., Co–Pd/BiVO₄: high-performance photocatalysts for the degradation of phenol under visible light irradiation. *Appl. Catal. B Environ.* **224**, 350–359 (2018). <https://doi.org/10.1016/j.apcatb.2017.10.044>
37. S. Singh, R. Sharma, M. Khanuja, A review and recent developments on strategies to improve the photocatalytic elimination of organic dye pollutants by BiOX (X= Cl, Br, I, F) nanostructures. *Korean J. Chem. Eng.* **35**, 1955–1968 (2018). <https://doi.org/10.1007/s11814-018-0112-y>
38. M.H. Abdurahman, A.Z. Abdullah, W. Da Oh et al., Tunable band structure of synthesized carbon dots modified graphitic carbon nitride/bismuth oxychlorobromide heterojunction for photocatalytic degradation of tetracycline in water. *J. Colloid Interface Sci.* **629**, 189–205 (2023). <https://doi.org/10.1016/j.jcis.2022.08.172>
39. Y. Tang, W. Wang, B. Wang et al., A novel AgCl-based visible-light photocatalyst through in-situ assembly of carbon dots for efficient dye degradation and hydrogen evolution. *Sustain. Mater. Technol.* **27**, e00242 (2021). <https://doi.org/10.1016/j.susmat.2020.e00242>
40. H. Yu, R. Shi, Y. Zhao et al., Alkali-assisted synthesis of nitrogen deficient graphitic carbon nitride with tunable band structures for efficient visible-light-driven hydrogen evolution. *Adv. Mater.* **29**(16), 1605148 (2017). <https://doi.org/10.1002/adma.201605148>
41. C.Y. Wang, X. Zhang, H.B. Qiu et al., Photocatalytic degradation of bisphenol A by oxygen-rich and highly visible-light-responsive Bi₁₂O₁₇Cl₂ nanobelts. *Appl. Catal. B Environ.* **200**, 659–665 (2017). <https://doi.org/10.1016/j.apcatb.2016.07.054>
42. B. Parasuraman, B. Kandasamy, I. Murugan et al., Designing the heterostructured FeWO₄/FeS₂ nanocomposites for an enhanced photocatalytic organic dye degradation. *Chemosphere* **334**, 138979 (2023). <https://doi.org/10.1016/j.jhazmat.2020.122670>
43. X. Wang, L. Jiang, K. Li et al., Fabrication of novel Z-scheme SrTiO₃/MnFe₂O₄ system with double-response activity for simultaneous microwave-induced and photocatalytic degradation of tetracycline and mechanism insight. *Chem. Eng. J.* **400**, 125981 (2020). <https://doi.org/10.1016/j.cej.2020.125981>
44. Y. Chi, S. Xu, M. Li et al., Effective blockage of chloride ion quenching and chlorinated by-product generation in photocatalytic wastewater treatment. *J. Hazard. Mater.* **396**, 122670 (2020). <https://doi.org/10.1016/j.jhazmat.2020.122670>
45. S. Yang, D. Xu, B. Chen et al., In-situ synthesis of a plasmonic Ag/AgCl/Ag₂O heterostructures for degradation of ciprofloxacin. *Appl. Catal. B Environ.* **204**, 602–610 (2017). <https://doi.org/10.1016/j.apcatb.2016.10.013>
46. W. Zhang, Y. Liang, Y. Sun et al., Ag/AgCl nanoparticles assembled on BiOCl/Bi₁₂O₁₇Cl₂ nanosheets: enhanced plasmonic visible light photocatalysis and in situ DRIFTS investigation. *Appl. Surf. Sci.* **455**, 236–243 (2018). <https://doi.org/10.1016/j.apsusc.2018.05.171>

Publisher's Note Springer Nature remains neutral with regard to jurisdictional claims in published maps and institutional affiliations.

Springer Nature or its licensor (e.g. a society or other partner) holds exclusive rights to this article under a publishing agreement with the author(s) or other rightsholder(s); author self-archiving of the accepted manuscript version of this article is solely governed by the terms of such publishing agreement and applicable law.